Title
Local Fluxionality of Surface-Deposited Cluster Catalysts: The Case of Pt7 on Al2O3

Journal
The Journal of Physical Chemistry Letters, 9(7)

ISSN
1948-7185

Authors
Zhai, Huanchen
Alexandrova, Anastassia N

Publication Date
2018-04-05

DOI
10.1021/acs.jpclett.8b00379

Peer reviewed

Local Fluxionality of Surface-Deposited Cluster Catalysts: the Case of Pt_7 on Al_2O_3

Huanchen Zhai,[1] and Anastassia N. Alexandrova[1,2,*]
[1]*Department of Chemistry and Biochemistry, University of California, Los Angeles, Los Angeles, California 90095, United States*
[2]*California NanoSystems Institute, Los Angeles, California 90095, United States*
*Corresponding Author: E-mail: ana@chem.ucla.edu

Abstract

Sub-nano surface-supported catalytic clusters, can be generally characterized by many low-energy isomers accessible at elevated temperatures of catalysis. The most stable isomer may not be the most catalytically active. Additionally, isomers may interconvert across barriers, i.e. exhibit fluxionality, during catalysis. To study the big picture of the cluster fluxional behavior, we model such a process as isomerization graph using bipartite matching algorithm, harmonic transition state theory, and paralleled nudged elastic band method. All the minimal energy paths form a minimum spanning tree (MST) of the original graph. Detailed inspection shows that, at temperatures typical for catalysis, the cluster geometry changes frequently within several regions in the MST, while transition across regions is less likely. As a further confirmation, the structural similarity analysis was additionally performed based on molecular dynamics trajectories. This local fluxionality picture provides a new perspective on understanding finite-temperate catalytic processes.

TOC graphics

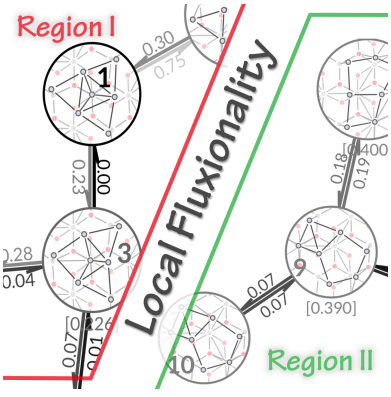

Surface-supported transition metal clusters are attractive materials for heterogeneous catalysis. Many experimental and theoretical studies have been conducted on this topic recently.[1] Small (sub-nano) clusters often appear to be more interesting than bigger ones, in terms of their catalytic activity and selectivity.[2] However, most of their properties are "non-scalable" with cluster size, and that raises

many difficulties when traditional computational methods are applied to study these systems. Using global optimization algorithms[3-5] combined with density functional theory (DFT), the potential energy surface (PES) of such systems can be explored, from which the geometric and electronic structures of some of the low-energy isomers of surface-supported sub-nano clusters can be identified and studied. However, many important finite-temperature effects, such as cluster isomerization process[6,7], cannot be derived simply from the static (thermodynamic) isomer representation[4]. The kinetics of cluster isomerization is another important component contributing to the accessible system dynamics. However, finding efficient computational methods to study these dynamic effects remains a challenge.

In this work we use as example the Pt clusters deposited on α-alumina, of interest to catalytic dehydrogenation. A particularly interesting cluster size regime is around seven or eight Pt atoms, where special catalytic activity was observed.[2,8,9] In catalytic dehydrogenation of ethylene, for example, Pt_7 on α-Al_2O_3 showed a special activity.[8] Clusters of this size have a significant number of isomers, the number of which grows exponentially as the number of atoms increases.[4] But only a few of these isomers are low enough in energy to be thermally accessible at temperatures of dehydrogenation (400-600 K).[8] And a comprehensive view of the isomerization process will help us understand cluster fluxional behavior, which is believed to play an important role in catalysis.[10,11]

Recently, some novel computational methods have been developed for investigating the isomerization process of molecules and clusters. Anharmonic downward distortion following (ADDF)[6,12] and reactive global optimization (RGO)[13] are low-frequency modes searching based methods, which have been successfully applied to gas phase systems and heterogeneous system, where for the later case the surface is approximately represented by point charges.[13] However, it is known that the surface can form directional and strong bonds to the atoms of the cluster, and thus greatly impact the cluster geometry, electronic structure, and stability. Hence, both the surface and the cluster need to be represented accurately. In this case, the existing methods become inefficient, since they cannot be applied to large systems, particularly because of the computational expense of the vibrational frequency calculations (based on finite difference algorithm). An alternative is a two-step scheme, where the low-energy isomers are first obtained from global optimization, and then the transition paths between each pair of these isomers can be calculated, for example using the nudged elastic band (NEB) method.[14] Since NEB calculations are completely uncoupled, the scheme can be highly parallelized. This is the basic computational framework used in this work.

However, one major problem still exists for studying a cluster like Pt_7, or any other system that consists of many atoms of the same element. For a given pair of two different isomers, determination of an initial "guessed" path as the staring point of NEB will no longer be trivial. To determine an initial path, a matching (hereafter "atomic matching") between atoms of the two isomers (namely, a map from the atomic indices of isomer *A* to the atomic indices of isomer *B*) has to be established. Then, the coordinates of intermediate structures along the path can be calculated by linear interpolation between coordinates of every pair of matched atoms. If the atomic matching is not optimal, the minimal energy path (MEP)[15] given by converged NEB generally will not be optimal either. For example, in Fig. 1 we show two possible paths that connect the isomers #19 and #11 that resulted from a global optimization run. For every pair of Pt_7 isomers, the number of possible atomic

matches is 7! = 5040. Obviously, it is computationally unaffordable to traverse all these possible matches to find the optimal isomerization path. (Note that here we do not consider the matching of surface atoms. We assume that the displacement relative to their individual equilibrium positions is small for surface atoms, so that surface atoms will directly match to the closest surface atoms in the other isomer.)

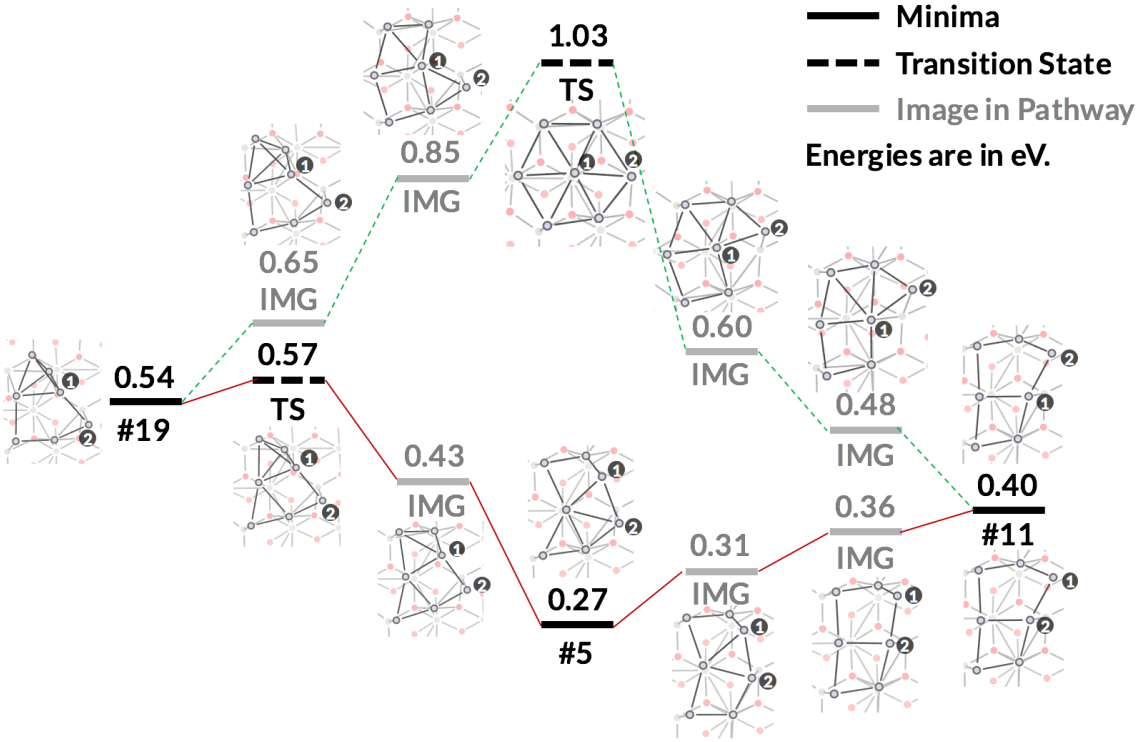

Figure 1. The two pathways of isomerization from the isomer #19 to the isomer #11 (numeration comes from the global optimization, starting from the global minimum as isomer #1), with different atom matching schemes. The atoms that move significantly during isomerization are labeled as 1 and 2 in the isomer #19. Along the upper pathway (green dashed lines), atom 1 goes towards center. Along the lower pathway (red solid lines), atom 1 goes away from center. It turns out that the second pathway has a much lower barrier height. Black circles, red dots, and brown dots represent Pt, O, and Al atoms, respectively.

One possible solution is performing NEB calculations only for "promising" atomic matching. We define the difference between the geometry of two isomers i, j as

$$\Delta_{ij} = \frac{1}{n} \min_{\hat{S}\in \mathrm{G(surf)}} \min_{\hat{P}\in P_n} \sum_{k=1}^{n} \left\| \left(\hat{S}\hat{P}\boldsymbol{x}^i\right)_k - \boldsymbol{x}_k^j \right\| \equiv \min_{\hat{P}\in P_n} \Delta_{ij}\left(\hat{P}\right) \qquad (1)$$

where n is the number of atoms in the cluster (for Pt_7, n = 7), G(surf) is the subgroup of the space group of the support material (in this work, Al_2O_3), including only those symmetric transforms, namely, $\hat{S}$, that keep z coordinates invariant, P_n is the set of all permutations $\hat{P}$ of a sequence 1,2, …, n, $\boldsymbol{x}_k^j$ is the x,y,z coordinates (as a vector) of the kth atom in isomer j, and $\|\cdot\|$ denotes the 2-norm of a vector, which is also the Euclidean length of the vector. The geometric difference Δ_{ij} defined by Eq. (1) is a measurement of linear Euclidean distance between two isomers based on optimal symmetry transformations, which is also known as root-mean-square distance (RMSD)

between the two isomers.[16] If the structural difference Δ_{ij} is directly evaluated using Eq. (1), the time complexity will be O(n!), which is non-polynomial. We propose to evaluate this using an efficient matching algorithm in graph theory, called Kuhn-Munkres (KM) algorithm,[17,18] which has been widely applied and adapted to similarity measurement and alignment problem of gas phase clusters.[16,19-22] There are two major differences between the KM algorithm implementation adapted for this work and previous gas-phase-focused applications: (i) the RMSD Δ_{ij} is minimized over symmetry operations related the space group of the support material, as shown in Eq. (1); (ii) not only the optimal, but also sub-optimal atomic matches are used for MEP optimization, as explained below. A weighted bipartite can be denoted as $B = (X, Y, E, W)$, where X and Y are two vertex sets satisfying that $|X| = |Y| = n$, $E \subseteq X \times Y$ is edge set (in this work we always have $E = X \times Y$), and $W: E \rightarrow \mathbb{R}$ defines weights of all edges. A matching M is a subset of edges no two of which share a common vertex. A matching M is best if $|M| = n$ and the sum of weights of edges in M is minimal. The bipartite model for solving cluster atomic matching is demonstrated in Fig. 2. We further assume that if the MEP between two isomers is a direct path (without any intermediates), the geometry of the two isomers must be similar enough. This assumption is based on the following argument. The actual distance measured along MEP (MEP distance) is at least as long as the linear distance defined in Eq. (1). Therefore, the MEP distance is generally long for isomers with large Δ_{ij}. Under this case, either there will be more likely some intermediates along the MEP, or the energy barrier of a direct transition will possibly be high. Then it is reasonable to consider only k permutations $\hat{P}$ of atomic indices, which gives k minimal $\Delta_{ij}(\hat{P})$, where k is a small constant. Kuhn-Munkres algorithm finds k best solutions for bipartite matching with $O\left((k+\sqrt{n})n^2\right)$ time complexity (k is set to 4 in this work). This means that the value of $\min_{\hat{P}\in P_n} \sum_{k=1}^{n} \left\| \left(\hat{S}\hat{P}\boldsymbol{x}^i\right)_k - \boldsymbol{x}_k^j \right\|$ and the corresponding $\hat{P}$ in Eq. (1) can be evaluated in polynomial time.

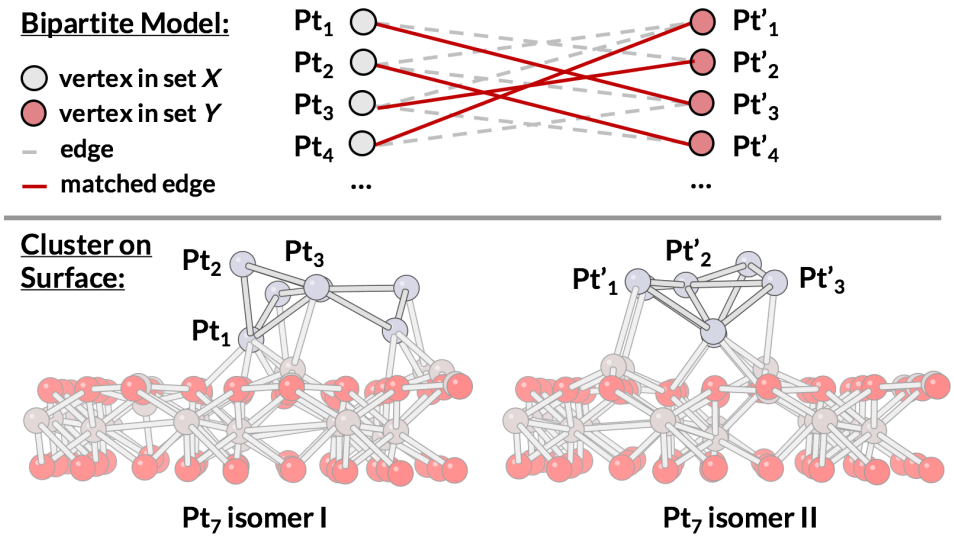

Figure 2. We model the atoms in two isomers as vertices in two sub-graphs (X and Y) in the bipartite graph, and the weights of edges are defined by the Euclidean distances between each of all possible pairs of the atoms. Using Kuhn-Munkres algorithm, we are able to find the best correspondence of atoms, which gives the smallest mean of

displacements over all matched pairs of atoms.

The alumina surface support is modeled as a 3×3 unit cell slab model, with lattice constants a = 4.807 Å and c = 13.117 Å. To find all relevant Pt_7 isomers (local minima) with surface-cluster interaction fully considered, the Basin Hopping (BH) method[23] is used, with the electronic structure calculations performed by plane wave density function theory (DFT) implemented in Vienna Ab initio simulation package (VASP) 5.4.1.[24-26] In BH method, 10 paralleled Monte Carlo (MC) walkers are initiated, each performing 200 moves, at temperature 1,500 K. Initial structures are generated using second-order Bond Length Distribution Algorithm (BLDA).[4] The 30 low-energy local minima (considered as isomers) are shown in Supporting Information Table S1.

In order to study the cluster isomerization at the temperature that is typical for catalysis (about 700 K), we consider isomers with energy less than 0.6 eV. Using similarity measurement Eq. (1), we can now calculate pathway between pairs of isomers with Δ_{ij} lower than a threshold (in this work, 1.5 Å) by NEB optimization. For each pair, if there are multiple $\hat{P}$ satisfying $\Delta_{ij}(\hat{P}) < 1.5$ Å, at most four different $\hat{P}$ that give relatively lower $\Delta_{ij}(\hat{P})$ will be used. Some additional higher-energy isomers are found to be intermediates along the transition paths between these low-energy isomers, and they are also included in Table S1. Based on NEB optimized MEP, an isomerization graph (Supporting Information Fig. S1) can be constructed. Isomers are represented as vertices. If the optimized path contains no intermediates (a direct path), it corresponds to an edge in the graph; otherwise, it corresponds to a path in the graph. When only edges in MEP are retained in the graph, the graph becomes a tree (a tree is a connected n-vertex graph with $n - 1$ edges) shown in Fig. 3. The energy and geometry of transition states in direct paths are shown in Supporting Information Table S2. An alternative way to visualize the connection between isomers is the disconnectivity graph[27] shown in Supporting Information Fig. S2. For every direct path, according to harmonic transition state theory (HTST) the rate constant for isomer transition is estimated to be[14]

$$k_{\mathrm{HTST}} = \frac{\prod_i^{3N} \nu_i^{\mathrm{init}}}{\prod_i^{3N-1} \nu_i^{\mathrm{TS}}} \mathrm{e}^{-\frac{E^{\mathrm{TS}} - E^{\mathrm{init}}}{k_B T}} \qquad (2)$$

where N is the total number of atoms, including cluster atoms and upper half of the surface atoms (which are not fixed during the relaxation, N = 7 (cluster) + 135 (surface) = 142 in this work). ν_i^{init} and ν_i^{TS} are frequencies of the vibrational normal modes at the initial state and transition state, respectively. E^{init} and E^{TS} are energies of the two states, respectively. The rate constants are evaluated at 450 K and 700 K and listed in Supporting Information Table S3. We note that in HTST harmonic approximation of the PES has been made in the vicinity of isomers and transition states. This makes HTST suitable for probing finite temperature effects, which are not included in simple local minima representation of the PES.

It is shown in Fig. 3 and Table S3 that transition barrier (along MEP) varies from 0.0004 eV to 0.7771 eV. In addition, there are some regions in the graph where the transition rate constant between adjacent isomers is relatively high (greater than 5.0×10^{10} s^{-1}) at 700 K (which typically corresponds to low energy barrier), for example, isomers #1, #3, #6, #16, and #24 form region I,

while isomers #2, #4, #5, #7, #18, etc. form region II (See Supporting Information Figs. S3 and S4). The two separated regions can also be clearly identified in disconnectivity graph (Supporting Information Fig. S2). Note that the number of isomers that should be included in each region also has dependence on temperature. More importantly, if we consider a "local interval" in time axis (with time span less than 1 ns), the cluster isomerization will also happen in a "local" region in configuration space, consisting of only structures of similar shape. For example, the rate constant for transition from isomer #3 to isomer #1 (with in region I) is 1.07×10^{13} s^{-1}, which is much higher than the rate 9.65×10^{7} s^{-1} transition from isomer #1 to isomer #15 (leaving region I). The region boundaries at 450 K are similar but more contracted. We further note that the RMSD between isomers in the same region is very small (for example, RMSD between isomer #1 and isomer #3 is 0.26 Å), while the RMSD between isomers in different regions is much larger (for example, RMSD between isomer #1 and isomer #2 is 2.71 Å). However, the energies of isomers #1 and #2 only differ by 0.0727 eV, and they form two "basins" (regions in Fig. 3) attracting higher-energy isomers with similar shapes. But the two "basins" are separated by high-energy barrier due to the large difference in geometry between isomers #1 and #2. This gives a "local fluxionality" picture of cluster isomerization at a finite temperature. The two regions also feature differences in the electronic structure of the clusters. As discussed in Ref. 9, the family of the isomers in Region I (including the global minimum) feature more prismatic, globular shapes, while species in Region II (containing the second lowest-energy isomer) have more open, or single-layer geometries. Species of Region II exhibit greater charge transfer from the support to the cluster, and that makes them more prominent players in catalytic dehydrogenation than the more stable global minimum. Pt atoms in these cluster isomers additionally exhibit stronger intra-cluster polarization.

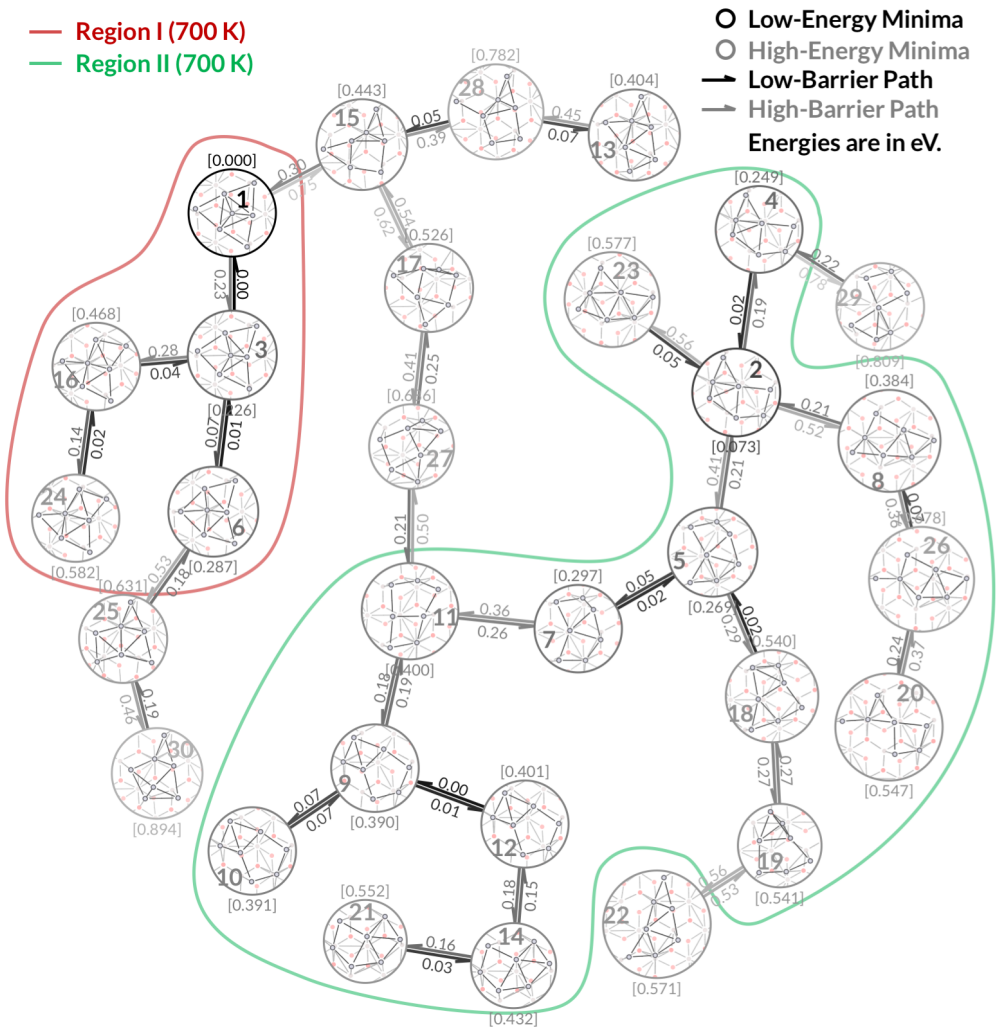

Figure 3. The minimal energy paths (MEPs) in the minimum spanning tree (MST) derived from isomerization graph. Isomers, transition paths, isomer energies and transition barrier energies are denoted as circles, arrows (edges), numbers in bracket and numbers on arrows, respectively. Isomers are labeled from 1(lowest energy, GM) to 30 (highest energy). In MST, there is a unique path between any two isomers, which represents the MEP between the two isomers. The rough boundaries of the region I and region II (discussed in text) are labeled in red and green, respectively.

To further examine the local fluxionality picture of isomerization of Pt_7 clusters, we performed molecular dynamics (MD) simulations. The MD simulation can properly include the effect of anharmonicity, which is missing in our isomerization graph build upon HTST. The NVT ensemble simulation is performed at 450 K and 700 K, respectively, for the 5.0 ps duration with the time step being 0.5 fs. A Nose-Hoover thermostat is used. The system was considered to be equilibrated after 0.5 ps, and after that time, information was collected. The geometry of the cluster part of the system at any moment of the simulation can be very different from the 0 K isomers, due to the complexity of PES and thermal expansion effect. To analyze the trajectories, Eq. (1) is used to measure the difference between geometry of the given cluster at every MD instant and geometries of several adjacent 0 K isomers. Fig. 4 (a) and (b) shows the trajectories starting from the isomer #1 simulated

at 450 K and 700 K, respectively. As the system evolves, the cluster loses its geometric identity, and may approach other isomers instead. It is shown that the (locally) equilibrated system is roughly a mixture of the isomers #1 and #3 at 450 K. The similarity to other isomers is small throughout the trajectory. However, when we simulate the system at 700 K, we can see much greater isomerization and geometric mixing, and, for example, at 3.9 ps of the trajectory the cluster is equidistant from the isomers #1, #3, #6, and #16. At this moment, the geometry is still far away from isomer #15 (with a distance of 1.0 Å). This implies that, at 700 K the locally fluxional region I (including isomers #1, #3, #6, and #16) may be a better representation of the system evolving from the isomer #1, than a fixed representation characterized by the geometry of isomer #1 alone. Similarly, Fig. 5(a) and (b) shows the trajectories starting from isomer #2 simulated at 450 K and 700 K, respectively. Although the energy of isomers #1 and 2 only differs by 0.072 eV, they are connected by a long path (including isomers #27, #17 and #15) with high barrier in isomerization MST and belong to different regions (Figure 3). It is shown that the system is fluxional among isomers #2, #4 and #5 at 450 K, and among #2, #4, #5, and #7 (all from region II) at 700 K, which are clearly indicated in Fig. 5(a) at 1.5 ps and Fig. 5(b) at 1.2 ps. This agrees with our previous analysis based on isomerization graph, and the regions I and II are actually connected subgraphs of the isomerization MST. This outcome is remarkable, because, in some cases of catalysis, it provides possible mechanism for the system to retain specific, highly active metastable states for some period of time. In the case of Pt_7, the timescale for local fluxionality is about 1 ns (estimated from the cross-region transition rate at 700 K).

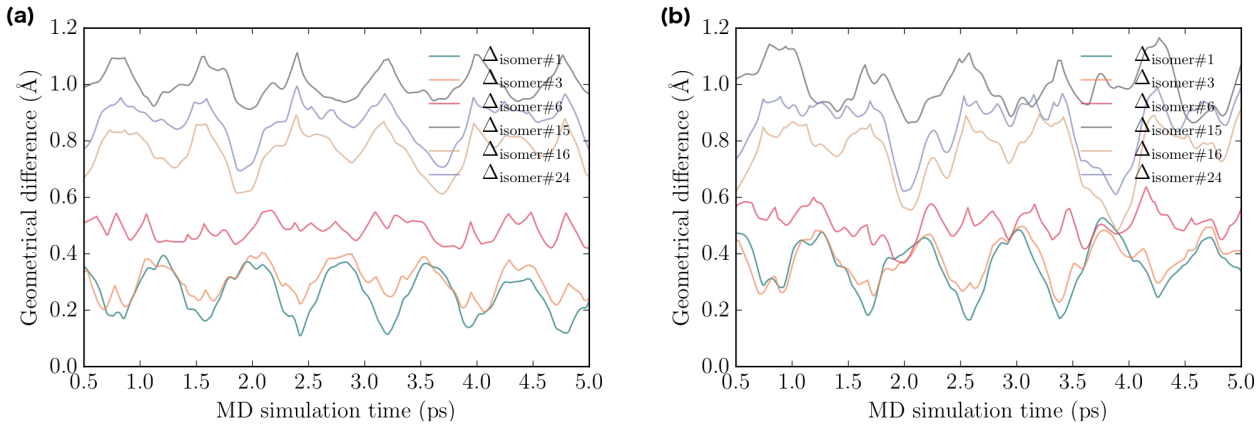

Figure 4. The MD trajectories starting from isomer #1 simulated at (a) 450 K and (b) 700 K. The trajectories from 0.0 to 0.5 ps are used to establish the equilibrium and thus not included in this figure. For trajectory at each temperature, the snapshot geometry at every time step is compared against several isomer geometries inside the region I (isomers #1, #3, #6, #16 and #24) and outside the region I (#15). The geometrical difference between two structures is defined in Eq. (1). Note that during the simulation, the position of surface atoms also changes. These (usually small) changes are not included in the evolution of Eq. (1).

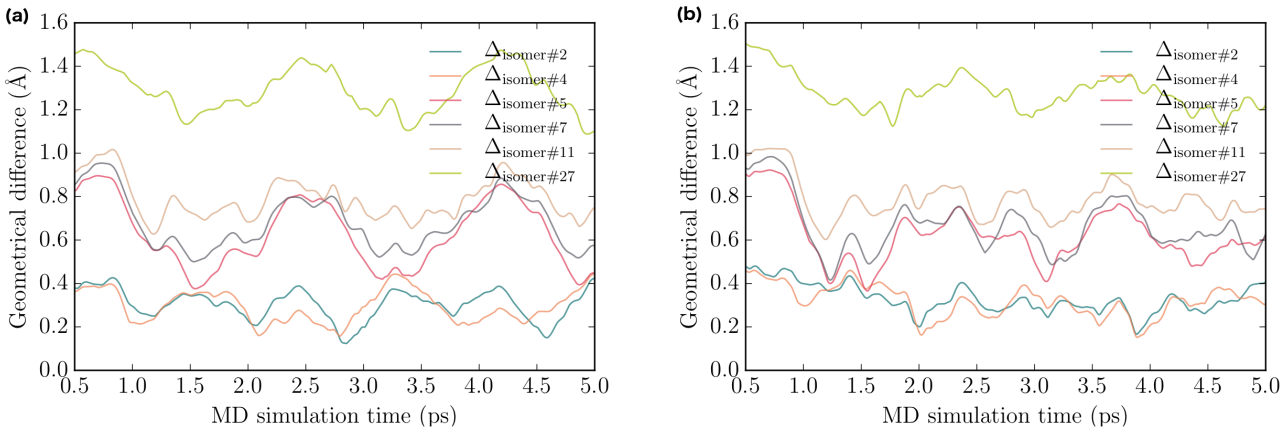

Figure 5. The MD trajectories starting from isomer #2 simulated at (a) 450 K and (b) 700 K. For trajectory at each temperature, the snapshot geometry at every time step is compared against several isomer geometries inside the region II (isomers #2, #4, #5, #7, #11) and outside the region II (#27). The geometrical difference between two structures is defined in Eq. (1).

Finally, detailed analysis on MD trajectories allows us to estimate anharmonicity effects in the system. We note that the geometries in MD are at least 0.11 Å far away from the isomer #1 or #2 at 450 K, and 0.17 Å far away from the isomer #1 or #2 at 700 K, respectively, which is a manifestation of the thermal expansion effect. In addition, there are some periodic patterns in Figs. 4 and 5, which indicate that some detailed comparison can be made between HTST rate constants and information extracted from MD simulations. From MD trajectories in Figs. 4 and 5, rate constants of the fastest process (namely, transitions between isomers #1 and #3 in region I and between isomers #2 and #4 in region II) can be approximately estimated by plotting the difference between the two lowest lines in Figures 4 and 5, and locating maxima and minima (Supporting Information Figs. S5 and S6). The rate constants estimated from HTST and MD trajectories for transition between these fast processes are summarized in Table 1. For transition between isomer #1 and #3, HTST predicts very different rates for the two directions, mainly due to the 0.226 eV energy difference between 0 K isomers #1 and #3. However, the geometrical difference between isomers #1 and #3 is only 0.26 Å. At finite temperature, the average electronic energies corresponding to these two isomer basins may become much closer as their geometries become more similar after thermal expansion. For transition between isomers #2 and #4, the MD predicted rates are close for the two directions as well, which is again explained by their very similar geometries. Finally, considering the nature and short duration of the MD simulation, we note that there are some important factors that may cause MD predicted rates listed in Table 1 to be inaccurate, as explained below. The vibrational frequencies of the cluster part of the system are ca. 50 cm^{-1} or 1.5 to 3.0 ps^{-1}, which can couple with the fast isomerization process. In addition, when several fast isomerization processes happen simultaneously, we cannot distinguish them by the simple analysis here. More accurate analysis should be based on free energy sampling methods, such as free energy perturbation,[28] umbrella sampling[29] and metadynamics,[30] which is beyond the scope of the work. To sum up, anharmonicity should be important for these fast processes because of the small geometrical difference between isomers and coupling between vibrational motion and isomerization process.

$\#_{init}$	$\#_{final}$	E_{init} (eV)	E_{TS} (eV)	T = 450 K	T = 700 K

				k_{HTST} (1/ps)	k_{MD} (1/ps)	k_{HTST} (1/ps)	k_{MD} (1/ps)
3	1	0.226	0.227	10.6	2.47	10.7	2.01
1	3	0.000	0.227	0.0337	2.33	0.272	3.08
4	2	0.249	0.267	14.7	1.54	17.2	1.47
2	4	0.073	0.267	3.56	1.20	21.3	2.02

Table 1. The electronic energies, HTST predicted rate constants and rate constants approximately estimated from MD trajectories for the fastest isomerization processes, namely, transition between isomers #1 and #3 and between isomers #2 and #4, in MD simulation starting from isomer #1 and #2, respectively.

In summary, in this work we build an isomerization graph of Pt_7 isomerization on α-alumina surface. A MST derived from this graph shows all MEPs of transition between any two Pt_7 isomers whose energies are below 0.6 eV, which are represented as vertices in the MST. We also introduced a structure difference measurement based on RMSD in cluster geometries and surface space group symmetry, and a fast polynomial algorithm based on bipartite model for efficient evaluation. This measurement is used to generate initial NEB paths and analyze MD trajectories. From both the HTST isomerization graph and MD trajectories, we find that the shape of surface supported Pt_7 isomers can be highly fluxional at finite temperature, with energy barriers of direct paths along MEP varying from ca. 0.00 eV to 0.78 eV. Based on our local fluxionality picture, the Pt_7 isomerization on α-alumina surface can be understood in two different timescales. The short time (less than 1 ns when T = 700 K) behavior can be described as frequent transitions among similar shapes within a local region, and the relatively longer time (greater than 1 ns when T = 700 K) behavior is the thermal equilibrium across regions. At lower temperature, the time span for local fluxionality can be much larger. For example, Yin *et al.* recently showed experimentally that the turn-over rate (TOR) of CO oxidation reaction catalyzed by Pt_{10} cluster supported on amorphous alumina is about 3000 CO_2 molecule per Pt_{10} cluster per second at 300 K.[31] If local fluxionality picture could also be valid for this system (which is unknown, after the realistic coverage of adsorbates are taken into consideration), assuming that the barrier height and imaginary frequency of "cross-region" transition were about 0.52 eV and ca. 50 cm^{-1}, respectively, the TOR would have the same order of magnitude as the rate of the "cross-region" transition, at this temperature. We note that this locally fluxional picture may have important implications for explaining catalytic mechanisms. The structurally similar isomers within each region share some common binding sites for reactant or product molecules. These common binding sites will exist for a relatively long time when the system only fluctuates locally (namely, within the region) but not globally. On the other hand, after considerably longer time the thermal equilibrium among all low-energy isomers will be achieved, which brings to question the reactivity on such clusters being considered at nearly fixed geometries (usually the global minimum).[32] An ensemble representation consisting of low energy isomers may be a better computational model for such occasions.[4,33]

Finally, the computational tools that we have developed for this work could be useful for studying isomerization or fluxionality of other cluster catalysts. Given the fact that the number of isomers within an energy range such as 0.6 eV may not be significantly larger for larger systems,[4,33] the cost of our approach should not increase dramatically. However, the realistic coverage and pressure may greatly change the potential energy surface,[33,34] and in this situation, whether or not the local

fluxionality picture is still valid is unknown. Our future work will be along this direction.

Acknowledgments

This work was supported by the Air Force Office of Scientific Research under a Basic Research Initiative grant (AFOSR FA9550-16-1-0141). CPU resources at the DoD High Performance Computing Modernization Program (AFRL DSRC, ERDC, and Navy DSRC), supported by the Department of Defense, Extreme Science and Engineering Discovery Environment's (XSEDE) computing resources, and UCLA-IDRE cluster were used to conduct this work.

The Supporting Information is available free of charge on the ACS Publications website: List of the 30 lowest-energy isomers of Pt_7 supported on α-Al_2O_3; list of transition states; table of rate constants and barriers; isomerization graph with MEP and non-MEP paths; disconnectivity graph; examples of NEB paths connecting pairs of isomers; details on estimation of rate constants from MD simulation; and computational details.

References

(1) Tyo, E. C.; Vajda, S. Catalysis by Clusters with Precise Numbers of Atoms. *Nat. Nanotechnol.* **2015**, *10*, 577–588.

(2) Vajda, S.; Pellin, M. J.; Greeley, J. P.; Marshall, C. L.; Curtiss, L. A.; Ballentine, G. A.; Elam, J. W.; Catillon-Mucherie, S.; Redfern, P. C.; Mehmood, F.; Zapol, P. Subnanometre Platinum Clusters as Highly Active and Selective Catalysts for the Oxidative Dehydrogenation of Propane. *Nat. Mater.* **2009**, *8*, 213–216.

(3) Davis, J. B. A.; Shayeghi, A.; Horswell, S. L.; Johnston, R. L. The Birmingham Parallel Genetic Algorithm and Its Application to the Direct DFT Global Optimisation of Ir_N (N = 10–20) Clusters. *Nanoscale* **2015**, *7*, 14032–14038.

(4) Zhai, H.; Alexandrova, A. N. Ensemble-Average Representation of Pt Clusters in Conditions of Catalysis Accessed through GPU Accelerated Deep Neural Network Fitting Global Optimization. *J. Chem. Theory Comput.* **2016**, *12*, 6213–6226.

(5) Jørgensen, M. S.; Groves, M. N.; Hammer, B. Combining Evolutionary Algorithms with Clustering toward Rational Global Structure Optimization at the Atomic Scale *J. Chem. Theory Comput.* **2017**, *13*, 1486–1493.

(6) Gao, M.; Horita, D.; Ono, Y.; Lyalin, A.; Maeda, S.; Taketsugu, T. Isomerization in Gold Clusters upon O_2 Adsorption. *J. Phys. Chem. C* **2017**, *121*, 2661–2668.

(7) Zhai, H.; Alexandrova, A. N. Fluxionality of Catalytic Clusters: When It Matters and How to Address It. *ACS Catal.* **2017**, *7*, 1905–1911.

(8) Baxter, E. T.; Ha, M.-A.; Cass, A. C.; Alexandrova, A. N.; Anderson, S. L. Ethylene Dehydrogenation on $Pt_{4,7,8}$ Clusters on Al_2O_3 : Strong Cluster Size Dependence Linked to Preferred Catalyst Morphologies. *ACS Catal.* **2017**, *7*, 3322–3335.

(9) Ha, M. A.; Baxter, E. T.; Cass, A. C.; Anderson, S. L.; Alexandrova, A. N. Boron Switch for Selectivity of Catalytic Dehydrogenation on Size-Selected Pt Clusters on Al_2O_3. *J. Am. Chem. Soc.* **2017**, *139*, 11568–11575.

(10) Häkkinen, H.; Abbet, S.; Sanchez, A.; Heiz, U.; Landman, U. Structural, Electronic, and Impurity-Doping Effects in Nanoscale Chemistry: Supported Gold Nanoclusters. *Angew. Chemie Int. Ed.* **2003**, *42*, 1297–1300.
(11) Xing, X.; Li, X.; Yoon, B.; Landman, U.; Parks, J. H. Dynamic Fluxionality and Enhanced CO Adsorption in the Presence of Coadsorbed H_2O on Free Gold Cluster Cations. *Int. J. Mass Spectrom.* **2015**, *377*, 393–402.
(12) Satoh, H.; Oda, T.; Nakakoji, K.; Uno, T.; Tanaka, H.; Iwata, S.; Ohno, K. Potential Energy Surface-Based Automatic Deduction of Conformational Transition Networks and Its Application on Quantum Mechanical Landscapes of D-Glucose Conformers. *J. Chem. Theory Comput.* **2016**, *12* (11), 5293–5308.
(13) Negreiros, F. R.; Aprà, E.; Barcaro, G.; Sementa, L.; Vajda, S.; Fortunelli, A. A First-Principles Theoretical Approach to Heterogeneous Nanocatalysis. *Nanoscale* **2012**, *4*, 1208.
(14) Henkelman, G. Atomistic Simulations of Activated Processes in Materials. *Annu. Rev. Mater. Res.* **2017**, *47*, 199–216.
(15) Koehl, P. Minimum Action Transition Paths Connecting Minima on an Energy Surface. *J. Chem. Phys.* **2016**, *145*, 184111.
(16) Griffiths, M.; Niblett, S. P.; Wales, D. J. Optimal Alignment of Structures for Finite and Periodic Systems. *J. Chem. Theory Comput.* **2017**, *13*, 4914–4931.
(17) Kuhn, H. W. The Hungarian Method for the Assignment Problem. *Nav. Res. Logist. Q.* **1955**, *7*, 83–97.
(18) Fukuda, K.; Matsui, T. Finding All the Perfect Matchings in Bipartite Graphs. *Appl. Math. Lett.* **1994**, *7*, 15–18.
(19) Helmich, B.; Sierka, M. Similarity Recognition of Molecular Structures by Optimal Atomic Matching and Rotational Superposition. *J. Comput. Chem.* **2012**, *33*, 134–140.
(20) Allen, W. J.; Rizzo, R. C. Implementation of the Hungarian Algorithm to Account for Ligand Symmetry and Similarity in Structure-Based Design. *J. Chem. Inf. Model.* **2014**, *54*, 518–529.
(21) Wagner, A.; Himmel, H. J. ARMSD: A Comprehensive Tool for Structural Analysis. *J. Chem. Inf. Model.* **2017**, *57*, 428–438.
(22) Temelso, B.; Mabey, J. M.; Kubota, T.; Appiah-Padi, N.; Shields, G. C. ArbAlign: A Tool for Optimal Alignment of Arbitrarily Ordered Isomers Using the Kuhn-Munkres Algorithm. *J. Chem. Inf. Model.* **2017**, *57*, 1045–1054.
(23) Wales, D. J.; Doye, J. P. K. Global Optimization by Basin-Hopping and the Lowest Energy Structures of Lennard-Jones Clusters Containing up to 110 Atoms. *J. Phys. Chem. A* **1997**, *101*, 5111–5116.
(24) Kresse, G.; Furthmüller, J. Efficient iterative schemes for ab initio total-energy calculations using a plane-wave basis set. *Phys. Rev. B* **1996**, *54*, 11169-11186.
(25) Blöchl, P. E. Projector augmented-wave method. *Phys. Rev. B* **1994**, *50*, 17953-17979.
(26) Perdew, J. P.; Burke, K.; Ernzerhof, M. Generalized Gradient Approximation Made Simple. *Phys. Rev. Lett.* **1996**, *77*, 3865–3868.
(27) Wales, D. J. Energy Landscapes: Calculating Pathways and Rates. *Int. Rev. Phys. Chem.* **2006**, *25*, 237–282.
(28) Jorgensen, W. L.; Thomas, L. L. Perspective on Free-Energy Perturbation Calculations for Chemical Equilibria. *J. Chem. Theory Comput.* **2008**, *4*, 869–876.

(29) Torrie, G. M.; Valleau, J. P. Nonphysical Sampling Distributions in Monte Carlo Free-Energy Estimation: Umbrella Sampling. *J. Comput. Phys.* **1977**, *23*, 187–199.
(30) Barducci, A.; Bussi, G.; Parrinello, M. Well-Tempered Metadynamics: A Smoothly Converging and Tunable Free-Energy Method. *Phys. Rev. Lett.* **2008**, *100*, 020603.
(31) Yin, C.; Negreiros, F. R.; Barcaro, G.; Beniya, A.; Sementa, L.; Tyo, E. C.; Bartling, S.; Meiwes-Broer, K.-H.; Seifert, S.; Hirata, H.; et al. Alumina-Supported Sub-Nanometer Pt_{10} Clusters: Amorphization and Role of the Support Material in a Highly Active CO Oxidation Catalyst. *J. Mater. Chem. A* **2017**, *5*, 4923–4931.
(32) Campbell, C.; van Santen, R.; Stamatakis, M.; Collis, N.; Freund, H.-J.; Plaisance, C.; Sauer, J.; Garrett, B.; Gross, E.; Kotarba, A.; et al. Catalyst Design from Theory to Practice: General Discussion. *Faraday Discuss.* **2016**, *188*, 279–307.
(33) Sun, G.; Sautet, P. Metastable Structures in Cluster Catalysis from First-Principles: Structural Ensemble in Reaction Conditions and Metastability Triggered Reactivity. *J. Am. Chem. Soc.* **2018**, *140*, 2812–2820.
(34) Hu, C. H.; Chizallet, C.; Mager-Maury, C.; Corral-Valero, M.; Sautet, P.; Toulhoat, H.; Raybaud, P. Modulation of Catalyst Particle Structure upon Support Hydroxylation: Ab Initio Insights into Pd_{13} and Pt_{13}/γ-Al_2O_3. *J. Catal.* **2010**, *274*, 99–110.